NANO
LETTERS

2005
Vol. 5, No. 9
1658−1667

Amphiphilic Four-Helix Bundle Peptides Designed for Light-Induced Electron Transfer Across a Soft Interface

Shixin Ye,[†] Bohdana M. Discher,[‡] Joseph Strzalka,*[,†] Ting Xu,[†] Sophia P. Wu,[†] Dror Noy,[‡,||] Ivan Kuzmenko,[§] Thomas Gog,[§] Michael J. Therien,[†] P. Leslie Dutton,[‡] and J. Kent Blasie[†,⊥]

Department of Chemistry and Department of Biochemistry & Biophysics, University of Pennsylvania, Philadelphia, Pennsylvania 19104, and Complex Materials Consortium, Advanced Photon Source, Argonne National Lab, Argonne, Illinois 60439

Received March 21, 2005; Revised Manuscript Received July 8, 2005

ABSTRACT

A family of four-helix bundle peptides were designed to be amphiphilic, possessing distinct hydrophilic and hydrophobic domains along the length of the bundle's exterior. This facilitates their vectorial insertion across a soft interface between polar and nonpolar media. Their design also now provides for selective incorporation of electron donor and acceptor cofactors within each domain. This allows translation of the designed intramolecular electron transfer along the bundle axis into a macroscopic charge separation across the interface.

Cofactors confer function to many biological proteins. Permanently associated cofactors are referred to as prosthetic groups and include metal atoms, flavins, quinones, metalloporphyrins, and so forth. Artificial protein models (or "maquettes"), based on α-helical bundle structural motifs, can now be designed to incorporate biological cofactors, based on the "bioinspiration" provided by the known high-resolution structures of the cofactor's local environment within the generally much larger soluble protein or membrane protein.[1] They can also be designed *de novo*, that is, from first principles, which is especially important for the incorporation of nonbiological cofactors.[2] These robust maquettes are much more simple structurally, relative to the natural proteins from which they were derived. The interior of the artificial protein scaffolding can be used to control the position, orientation, and properties of the cofactor within the peptide.[3] The exterior of the scaffolding can be used to control the peptide's supramolecular assembly into sufficiently ordered nanophase materials. Their macroscopic properties derive at a minimum from the incoherent superposition of the designed molecular properties of the ensemble, with the possibility of generating coherent phenomena.

The first maquettes designed to incorporate prosthetic groups used amphipathic dihelices, which self-assembled in aqueous solution forming hydrophilic four-helix bundles.[1] The dihelices were made amphiphilic via attachment of hydrocarbon chains to their N-termini.[4] The alkylated dihelices could be vectorially oriented in Langmuir monolayers at an air−water interface with their helical axes normal to the interface at higher surface pressures.[5] This vectorial orientation could be maintained upon the Langmuir−Blodgett deposition of these monolayers onto the nonpolar alkylated surface of a solid inorganic substrate.[6] However, any vectorial function exhibited by the peptide's prosthetic groups, for example, electron transfer between metalloporphyrin prosthetic groups, would necessarily occur only on one side of the interface.

Recently, we have designed and characterized two related four-helix bundle maquettes that are amphiphilic; namely, they possess distinctly hydrophilic and hydrophobic domains along the length of the exterior of the bundle. This facilitates their vectorial insertion across a soft interface between polar and nonpolar media. The two peptides, designated as AP0 and AP1 (i.e., for Amphiphilic Protein n), respectively,[7,8] were designed to bind prosthetic groups only within their hydrophilic domain. Within the hydrophilic domain, each helix was amphipathic (i.e., possessing polar and nonpolar faces) designed to position polar amino acid residues on the exterior of the bundle and nonpolar residues on the interior with the exception of histidine residues at selected locations to bind metallo-porphyrin prosthetic groups via axial ligation.

---

* Corresponding author. E-mail: strzalka@sas.upenn.edu.
[†] Department of Chemistry, University of Pennsylvania.
[‡] Department of Biochemistry & Biophysics, University of Pennsylvania.
[§] Complex Materials Consortium.
[||] Current address: Structural Biology Department, Weizmann Institute of Science, Rehovot 76100, Israel.
[⊥] E-mail: jkblasie@sas.upenn.edu.

10.1021/nl050542k CCC: $30.25 © 2005 American Chemical Society
Published on Web 08/23/2005

Table 1. Primary Amino Acid Sequences of HP1 Maquette and Current AP Maquettes[a]

HP1[9]	Ac-CGGGEIWKQHEEALKKFEEALKQFEELKKL-CONH$_2$
AP0[7]	Ac-EIWKLHEEFLKKFEELLKLHEERLKKLLLLALLQLLLALLQLGGC-CONH$_2$
AP1[8]	Ac-SSDPLVVAASIIGILHFILWILDRGGNGEIFKQHEEALKKFE-CONH$_2$
AP2	Ac-IIMAIAMVHLLFFFEIWKEFEEALKKFEEALKEFEELKKL-CONH$_2$
AP3[13]	Ac-CGGGIIMAIAMVHLLFLFEIWKQFEEALKKFE-CONH$_2$

[a] Color code same as that in the legend of Figure 1.

Within their hydrophobic domains, based on membrane ion channels, each helix remained amphipathic, but was designed to possess nonpolar residues on the exterior of the bundle and some uncharged polar residues on the interior. Thus, the design reversed the polar and nonpolar faces of each amphipathic helix at the junction between the hydrophilic to the hydrophobic domain along the length of the four-helix bundle.

These amphiphilic four-helix bundle maquettes have now been substantially redesigned to also selectively incorporate electron donor and acceptor prosthetic groups within their hydrophobic domains. As in AP0 and AP1, the new peptides have hydrophilic domains composed of amphipathic helices. These were modeled on the amphipathic helix HP1.[9] Two heptads from the HP1 sequence were incorporated into AP3, whereas nearly the entire sequence of HP1, almost 4 heptads, with a couple of substitutions, was incorporated into AP2 (Table 1). Unlike the hydrophobic domain of AP0, the hydrophobic domains of both AP2 and AP3 peptides were modeled using two heptads of a hydrophobic helix, namely, cytochrome *b*'s transmembrane helix D from the cytochrome *bc*$_1$ complex.[10] This helix possesses only one polar residue, a histidine selectively located in the interior of the bundle to bind metallo-porphyrin prosthetic groups via axial ligation. Thus, in addition to possessing bis-histidylmetalloporphyrin binding sites at one (AP3) or two (AP2) positions of the sequence within the hydrophilic domain, the two new amphiphilic four-helix bundle maquettes also possess a bis-histidyl metalloporphyrin binding site at one position within their hydrophobic domain. This is a key development toward creating an artificial electron transfer chain across the interface between polar and nonpolar media because binding appropriate electron donor and acceptor cofactors at these sites would permit electron transfer along the long axis of the bundle. Furthermore, the ability of these amphiphilic bundles to form vectorially oriented ensembles at interfaces means that the electron-transfer properties of the individual molecules can be translated into a macroscopic property of the interface.

The results reported here focus primarily on the larger AP2 maquette because the main difference between AP2 and AP3 is in the length of the hydrophilic domain. The primary sequence of each helix and a structural model of the four-helix bundle maquette are shown in Figure 1. This model reflects the parallel (or syn) topology that the bundle assumes at the air/water interface. The particular sequence shown has

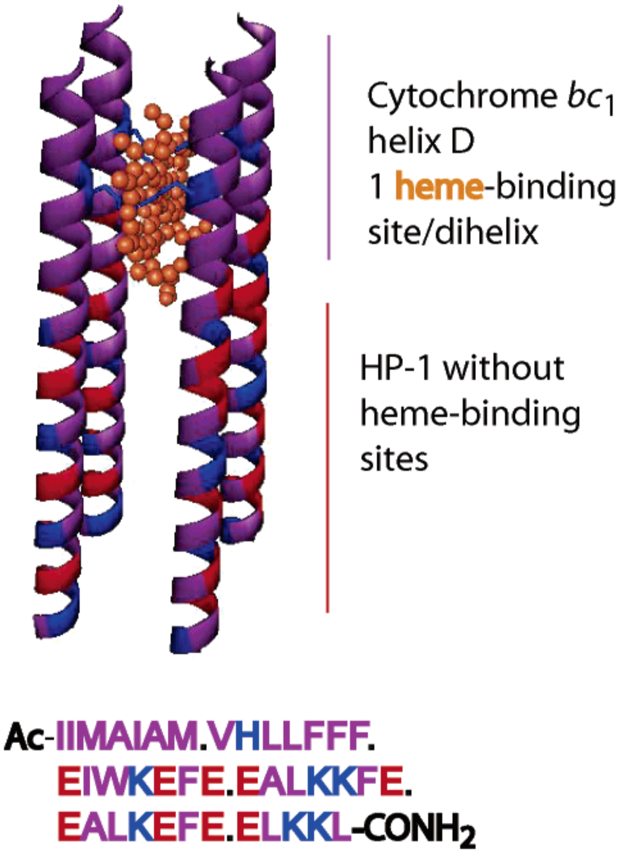

Figure 1. Schematic illustration of AP2 (purple, hydrophobic residues; blue, positively charged residues; red, negatively charged residues; and yellow, uncharged polar residues). The relatively hydrophilic but amphipathic HP1 sequence is elongated with two heptads of a more hydrophobic sequence taken from helix D of cytochrome bc1 complex. The helix D region is almost exclusively hydrophobic, except for histidine residues providing axial ligating sites from two adjacent helices for cofactor binding. Those histidine residues are presumably buried in the core region of the bundle. Four identical sequences self-assemble to form four-helix bundles in detergent micelles with a cofactor bound.

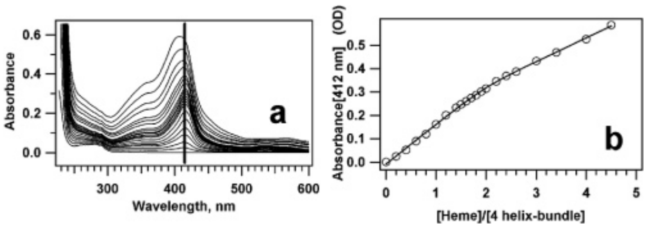

Figure 2. Titration of hemin into a 1.9 μM solution of apo-AP2 recorded in a 1-cm path-length cuvette. (a) Spectra shown contain 0.20, 0.40, 0.60, 0.80, 1.00, 1.20, 1.40, 1.50, 1.60, 1.70, 1.80, 1.90, 2.00, 2.20, 2.40, 2.60, 3.00, 3.40, 4.00, and 4.50 equiv of added hemin per four-helix bundle. A vertical-line at peak 412 nm indicates the blue shift of the peak with increasing hemin/peptide mole ratio, indicative of a contribution of free heme (absorption at 400 nm) in the solution at larger mole ratios. (b) Heme binding determined from the absorbance at 412 nm vs [heme]/[four helix bundle] ratio. The data are fit with a single dissociation constant of 60 nM, demonstrating that the binding is tighter than 100 nM.

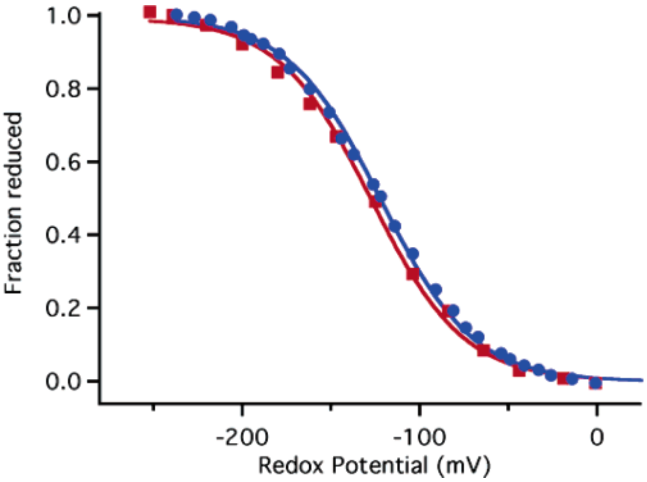

Figure 3. Oxidative (blue circles) and reductive (red squares) titration of AP2 peptide with two hemes bound per four-helix bundle measured at room temperature. The red and blue lines represent least-squares fits to $n = 1$ Nernst equation with midpoint potential of -122 and -127 mV, respectively. The sample contained 8 μM AP2 four-helix bundles in 100 mM KCl, 20 mM phosphate buffer, pH 8.0, with 0.9% OG.

only one hisitidine residue at sequence position 9 with phenylalanine replacing histidine at sequence position 20. This variation of AP2 facilitates the study of prosthetic group binding only within the hydrophobic domain of the amphiphilic four-helix bundle.

The primary sequence of AP2 is highly α-helical as shown by circular dichroism spectra in both methanol and buffered aqueous solutions containing the detergent *n*-octyl β-D-glucopyranoside (OG), namely, 77% and 71% helix content, respectively (data not shown). The helices of the AP2 sequence associate spontaneously to form a three-helix bundle, or an equilibrium mixture of two-helix and four-helix bundles, in their apo form, that is, in the absence of prosthetic groups, based on sedimentation equilibrium experiments indicating the average molecular weight of the sedimenting species to be intermediate between the expected values for two-helix and four-helix bundles. In the presence of stoichiometric concentrations of metalloporphyrin prosthetic groups, the helices of the AP2 sequence associate to form four-helix bundles based on the good agreement of their expected and experimentally determined molecular weights.

The affinity of the histidine site in the hydrophobic domain of the AP2 bundle in the detergent OG for binding metalloporphyrins is demonstrated via the titration of the peptide with the metalloporphyrin as monitored by optical absorption spectroscopy. The case for heme is shown in Figure 2 and analysis allowing for two such binding sites in the four-helix bundle demonstrates that the dissociation constant is less than 100 nM. The affinity for binding metalloporphyrin to histidyl sites within the hydrophobic domain of the AP2 four-helix bundle is comparable, within an order of magnitude, to the results reported for the closely related amphiphilic AP0 peptide (e.g., K_d's of <50 nM).[7] It is therefore anticipated that substituting His for Phe at position 20 or 27 of AP2 should give AP2 a second binding site in the hydrophilic domain with similar binding affinity. Oxidation−reduction titration of the AP2 peptide with two hemes per four-helix bundle shows that the two hemes titrate homogeneously with a single midpoint potential $E_m = -125 \pm 3$ mV without any hysteresis (Figure 3). The lack of interaction between the two hemes suggests that when solubilized with detergent, AP2 adopts an antiparallel (anti) topology, as would occur if the hydrophilic domain adopted the anti topology of the HP1 peptide on which it is based, and the hydrophobic domains and associated detergent molecules extended from either end of the bundle. By comparison, a single heme in a four-helix bundle of AP0 has a midpoint potential of -146 mV.[7]

In addition, the binding site in the hydrophobic domain of the AP2 four-helix bundle is capable of binding other prosthetic groups. For instance, AP2 can bind other porphyrin analogues that are much more hydrophobic than heme. One example is shown in Figure 4, which demonstrates the binding of a photosynthetic pigment, zinc-bacteriochlorophyll (ZnBChl), to AP2. A nickel-substituted BChl derivative (NiBChl) could also bind to AP2 (not shown) albeit with lower affinity. These hydrophobic BChl derivatives possess a 20-carbon long hydrocarbon side-chain[11,12] and therefore can bind to AP2's hydrophobic domain but not to the water-soluble HP1, the template for AP2's hydrophilic domain, or the amphiphilic AP0, with binding sites only in its hydrophilic domain. For a more detailed description of the interaction of these hydrophobic bacteriochlorophyll-based cofactors with the amphiphilic AP3 peptide, the reader is referred to another report.[13] The specificity of the binding site in the hydrophobic domain of AP2 for hydrophobic bacteriochlorophylls may allow their specific binding in the hydrophobic domain of AP2 and metallo-porphyrin within the (Phe → His substituted) hydrophilic domain.

AP2 (and AP0) are also capable of binding nonbiological prosthetic groups possessing much more extended π-electron systems. These can have the advantage of having the electron donor and the electron acceptor within the same prosthetic group[14] bound to the four-helix bundle via only a single bis-histidyl site. An example of such a prosthetic group is shown, symmetric in this instance, together with its anticipated location within AP2 in Figure 5; the hydrophobic domain

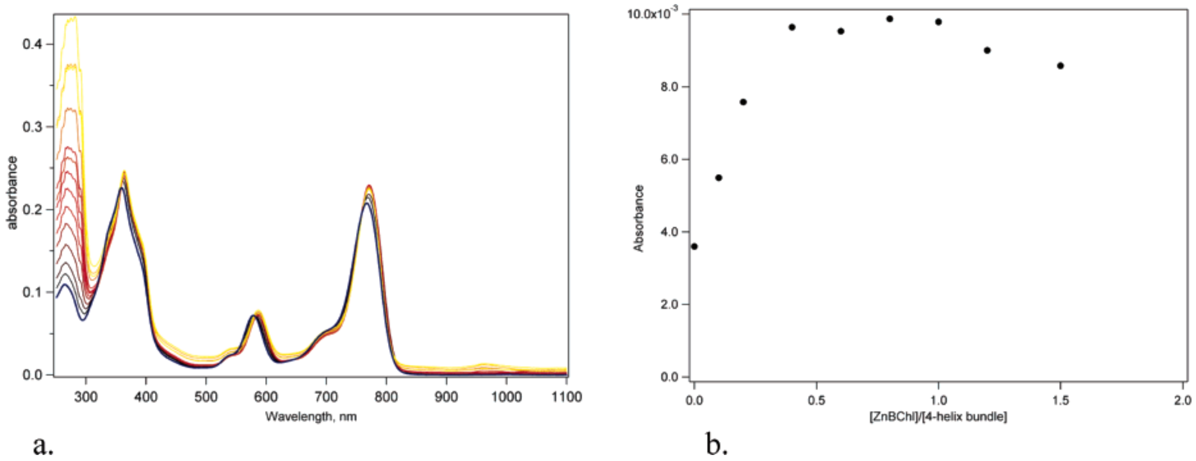

Figure 4. Absorbance spectra of ZnBChl in 0.9% OG, 50 mM KPi (solid blue), and titration with apo-AP2 in 4.5% OG, 50 mM KPi recorded in a 1-cm-path-length cuvette. (a) Spectra shown contain 0.10, 0.20, 0.40, 0.60, 1.00, 1.20, 1.50, 2.00, and 2.50 equiv of added Zn−BChl per four-helix bundle. The red shift (10 nm) of the peak at 580 nm indicates the axial ligation of ZnBChl by the histidines of AP2.[11,12] (b) ZnBChl binding determined from the absorbance at 590 nm vs [ZnBChl]/[four-helix bundle] ratio. The stoichiometry suggests saturation occurs within the range of 0.5−1.0 ZnBChl per four-helix bundle.

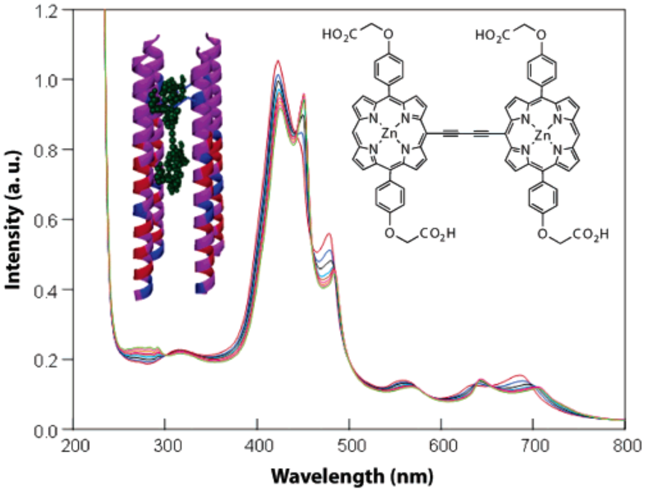

Figure 5. Binding of a distinctly nonbiological cofactor. The absorption spectrum of the "Zn33Zn" cofactor (inset on right: 5,5′-bis[(10,20-di-((4-carboxymethyleneoxy)phenyl)porphinato)zinc(II)]-butadiyne) solubilized with OG in a phosphate buffer changes as the apo-AP2 peptide is added. All features above 400 nm shift to the red upon peptide binding. The left inset shows a model of the cofactor−peptide complex. Coordination of only one of the two Zn-porphyrins at one end of the cofactor within the peptide's hydrophobic domain renders the otherwise symmetric chromophore asymmetric in the peptide environment.

of the bundle is shown in purple. The red shifts in the rich electronic spectrum of the prosthetic group, 5,5′-bis[(10,20-di-((4-carboxymethyleneoxy)phenyl)porphinato)zinc(II)]-butadiyne (abbreviated Zn33Zn), upon binding to the peptide via axial histidyl coordination[15−17] are also shown. The vectorial incorporation of this symmetric prosthetic group into the amphiphilic four-helix bundle AP2 (or AP0) via axial histidyl ligation of only a single Zn atom breaks the symmetry, to create an electronically asymmetric butadiyne-bridged bis(porphinato)zinc(II) chromophore. The resulting different redox potentials for the two Zn-porphyrins in the cofactor would thereby provide for light-activated electric charge separation across the interface.[14,18]

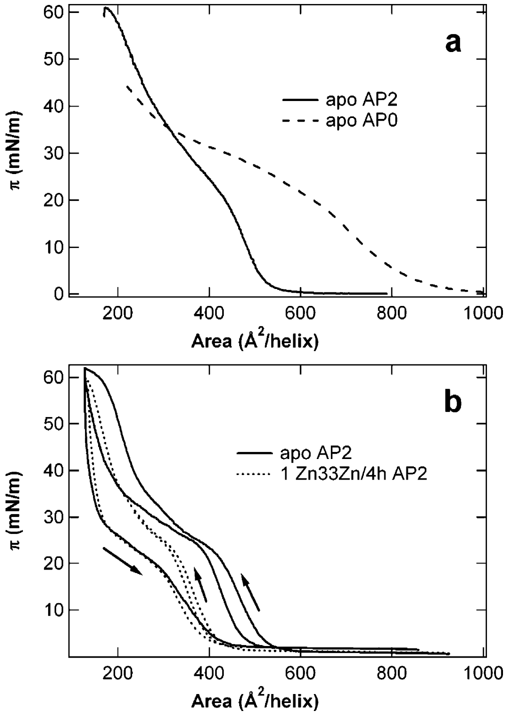

Figure 6. (a) Surface pressure−area isotherms of the pure peptide monolayers, apo AP2 (solid) and apo AP0 (dashed), both spread from methanol solution on a 1 mM phosphate/10 mM KCl buffer subphase, pH 8.0 at 20 °C. (b) Isotherms recorded for AP2 in the apo form (solid) and with 1 Zn33Zn bound per four-helix bundle (dotted) spread from aqueous solution with 0.45% OG detergent. Arrows indicate the compression or expansion of the monolayer.

Pressure−area isotherms recorded for Langmuir monolayers of the pure apo form of the amphiphilic AP2 are somewhat similar to those of the amphiphilic four-helix bundle maquette AP0,[7] as shown in Figure 6a. For areas/helix below 300 Å^2 upon compression, the surface pressure rises relatively steeply to a limiting value of about 55 mN/m at about 150−200 Å^2 for both apo-AP2 and apo-AP0. The relatively high surface pressures achieved at the minimal area/helix are indicative of AP2's amphiphilicity, as for AP0.

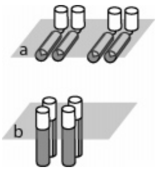

Figure 7. Schematic drawings of the AP2 peptide consistent with the isotherm and X-ray reflectivity data at low surface pressure (a) and at high surface pressure (b).

These minimal areas of about 180−200 Å^2/helix are about 2 times the estimated cross-sectional area of an ideal, perfectly straight α-helix oriented with its long axis perpendicular to the interface. For AP2 and areas/helix above 400 Å^2, the surface pressure decays to zero over the range 450−550 Å^2, whereas this occurs for AP0 at 700−800 Å^2. This may be explained by the fact that the helices of AP0 are amphipathic (i.e., possessing polar and nonpolar faces) over their entire length, whereas those for AP2 are amphipathic only over ~2/3 of their length, the remainder being exclusively hydrophobic over two heptads (14 residues). This hydrophobic portion would not be expected to lie in the plane of the interface and low surface pressures, unlike the case for amphipathic helices, and would more likely extend into the air above the water surface (Figure 7). This would reduce the average area/helix by ~210 Å^2 for AP2 as compared with AP0 at surface pressures below ~20 mN/m, assuming a rise/residue of 1.5 Å and a ~10 Å diameter for an α-helix. Comparison of the pressure−area isotherms for apo and holo forms of AP2 are shown in Figure 6b for the case of the Zn33Zn nonbiological cofactor. The isotherm for the holo form is shifted to smaller average areas/helix by as much as ~100 Å^2 for the lower surface pressures below 20 mN/m. This shift becomes progressively smaller at higher surface pressures, vanishing as the minimum average area/helix is approached at 55−60 mN/m. This shift in the lower pressure regime may be due to the ability of the cofactor to link two helices together via axial histidyl ligation of each Zn-porphyrin of Zn33Zn to a different helix, each containing only one histidine residue. This possibility is likely to vanish as the helices orient perpendicular to the interface at higher pressures forming four-helix bundles (see below). In addition, although the isotherms for both apo and holo forms of AP2 exhibit a pronounced hysteresis between compression and expansion, successive compression reproduces the features of the first compression, but at somewhat reduced area. This

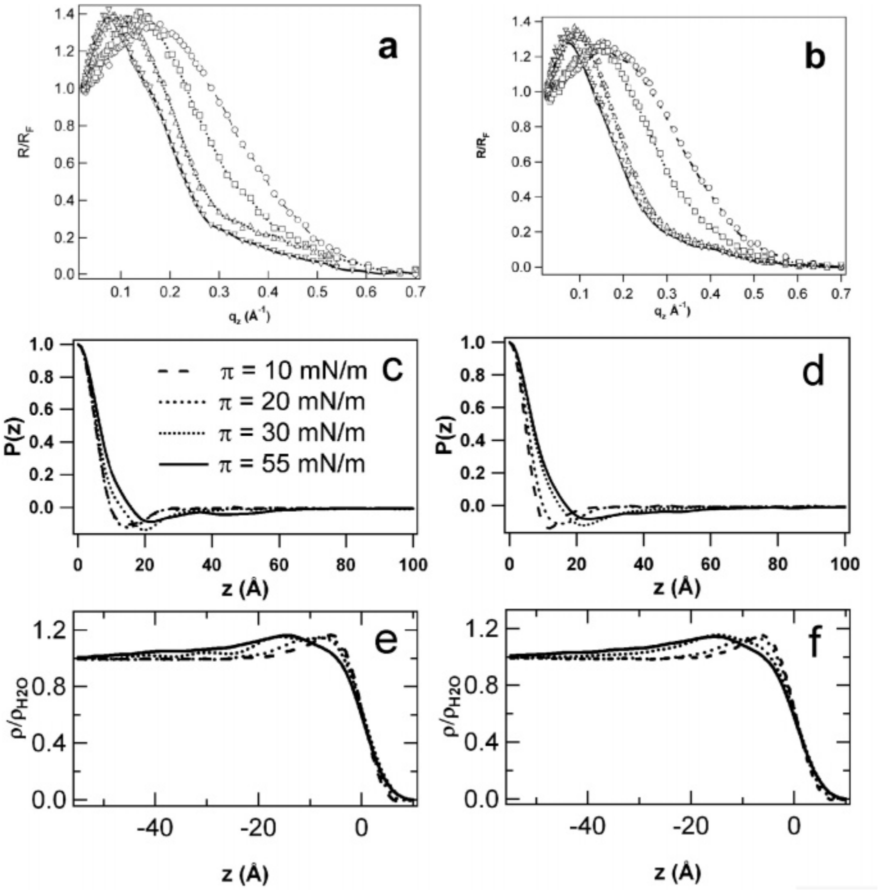

Figure 8. Fresnel-normalized X-ray reflectivity data collected from an apo-AP2 monolayer (a) and an AP2 monolayer with one heme/four-helix bundle (b) at surface pressures (π) of 10 (○), 20 (□), 30 (△), and 55 mN/m (▽). The continuous curves are calculated from the box-refinement result for the gradient profiles (not shown). (c) The Patterson or autocorrelation function of the monolayer gradient electron density profile computed from the data in a. (d) Patterson functions computed for a hemo-AP2 monolayer under conditions corresponding to those indicated in b. (e) The absolute electron density profiles for the apo-AP2 monolayer at each pressure computed by numerical integration of the gradient profiles from box refinement. (f) The absolute electron density profiles for the hemo-AP2 monolayer.

suggests that the four-helix bundles formed at the interface at higher surface pressures are indeed stable oligomeric forms.

With reference to the isotherms described above, normalized X-ray reflectivity data $R(q_z)/R_F(q_z)$ for the pure apo-AP2 peptide monolayer at four different pressures are shown in Figure 8a−b, the data being qualitatively similar to that for the holo form with the heme cofactor. At the lowest pressure of 10 mN/m, the data consist of a single broad maximum for momentum transfer $q_z < 0.7$ Å^{-1}. With increasing surface pressure, the maximum narrows and shifts to smaller q_z (developing subsidiary maxima/minima at the highest pressure investigated, near 55 mN/m, corresponding to 200 Å^2/helix). In Figure 8c−d, the inverse Fourier transforms of these data for both apo- and heme-AP2 are shown, which correspond to the autocorrelation of the gradient electron density profiles of the Langmuir monolayer at the four surface pressures. The gradient electron density profiles (not shown) were derived from the normalized reflectivity data via the box-refinement method, requiring no a priori assumptions, and Figure 8e−f shows the numerical integrals of these gradient profiles, namely, the electron density profiles of the monolayers of apo- and heme-AP2 at the four surface pressures. At the lower surface pressures of 10−20 mN/m, the electron density profiles for the apo- and heme-AP2 forms are consistent with the helices of AP2 self-associating to form dihelices with the long axis of each helix remaining parallel to the plane of the interface, but with the plane of the dihelix rotating to perpendicular to the plane of the interface resulting in the electron density profile of the monolayer approximately 20 Å in thickness, compared with that of ∼10 Å for a single helix, at 20 mN/m. At a pressure of 30 mN/m, some of the helices are starting to orient perpendicular to the interface, thereby penetrating ∼20 Å more deeply into the subphase. Finally, at a surface pressure of 55 mN/m, the electron density profile of the monolayer of both apo- and hemo-AP2 extends about 50 Å, being relatively uniform over the −40 to −5 Å region of the profile with the exception of a slight maximum at $z \approx -15$ Å. Considering the nature of the profiles for the monolayer at the lower pressures below 55 mN/m, this would be consistent with the long axis of the helices for a major fraction of the peptide in the monolayer, namely, about 95%, having become oriented perpendicular to the interface upon the pressure increase from 10 to 55 mN/m. Thus, the monolayer electron density profile at ∼55 mN/m is well-represented quantitatively by the weighted incoherent sum of the electron density profile for the AP2 helices oriented perpendicular to the monolayer plane and the profile for the AP2 helices oriented parallel to the monolayer plane, for example, the monolayer profile at ∼10 mN/m, the weighting factors given by the fractional areas occupied for each orientation in the monolayer plane. In this incoherent superposition, the minor fraction of helices lying parallel to the monolayer plane must be positioned in the monolayer profile at the air−water interface, namely, at the junction between the hydrophilic and hydrophobic domains of the helices lying perpendicular to the interface, namely, centered at $z \approx -15$ Å. Properly accounting for this superposition results in a profile for the AP2 helices being relatively uniform over their ∼50 Å length perpendicular to the monolayer plane. Overall, each helix of AP2 has 40 residues, which provide a length of ∼60 Å for a perfect straight

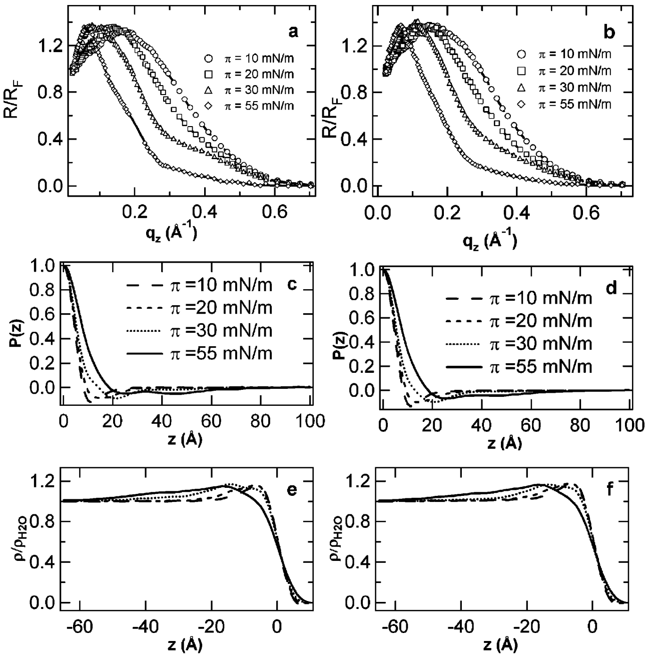

Figure 9. Fresnel-normalized X-ray reflectivity data for AP2 monolayers spread from aqueous buffer with 0.45% β-octyl glucoside in the apo form (a) and with two Zn33Zn cofactors bound per four-helices (b) at surface pressures (π) of 10 (○), 20 (□), 30 (△), and 55 mN/m (▽). The continuous curves are calculated from the box-refinement result for the gradient profiles (not shown). (c,d) The autocorrelation functions computed from the data in a and b, respectively. (e) The absolute electron density profile structures at each pressure obtained by numerical integration of the profile gradients for the apo AP2 monolayer. (f) The absolute electron density profiles for the monolayer of AP2 with Zn33Zn bound.

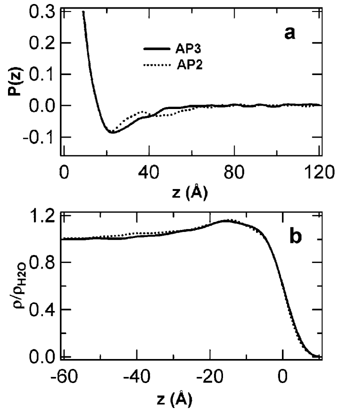

Figure 10. (a) Comparison of the autocorrelation functions computed from Fresnel-normalized X-ray reflectivity data for monolayers of apo AP2 (dotted) and apo AP3 (solid) spread from methanol solution and compressed to $\pi = 55$ mN/m. The function remains nonzero at larger z for the longer AP2 peptide. (b) The corresponding absolute electron density profiles for these monolayers calculated by numerical integration of the profile gradients from box refinement. The AP2 autocorrelation function and profile are the same as those shown in Figure 8.

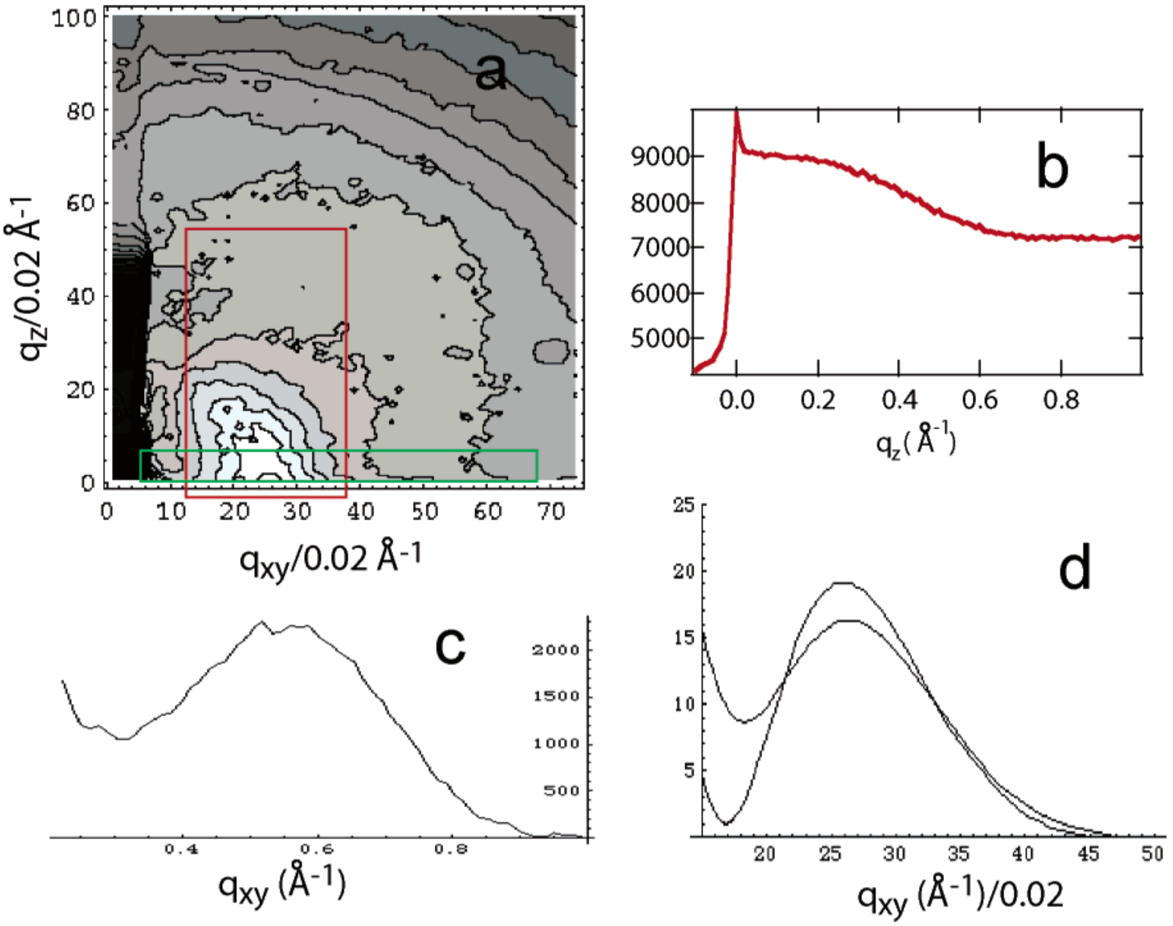

Figure 11. Grazing incidence X-ray diffraction (GIXD) from AP0 peptide monolayers. (a) Contour plot of 2D GIXD collected with a CCD area detector from a monolayer of apo-AP0 at high surface pressure. Integration of the region bounded by the red rectangle along q_{xy} gives the GIXD as a function of q_z (b), including background scattering. Integration of similar data from an apo-AP0 monolayer along the q_z direction (as indicated by the green box), after subtraction of otherwise equivalent GIXD from the pure subphase in the absence of the peptide monolayer, gives the background corrected GIXD as a function of q_{xy} (c). Model calculations for the q_{xy}-dependence of the in-plane diffraction from a bundle of four cylinders (d) show good agreement with the corrected data in (c), especially once the experimental Δq_{xy}-resolution is considered.

α-helix at 1.5 Å/residue along the long axis. The significant difference between the observed maximum thickness of the monolayer of ∼50 Å and the calculated length will be addressed later in this section. The interface between the hydrophobic domain of the peptide and air at ∼0 Å in these profiles is rather broad for both forms at this high surface pressure. The interface between the hydrophilic domain of the peptide and the pure aqueous subphase at −45 Å is more broad for the heme-AP2 than for the apo form (as also evidenced by the correspondingly more pronounced minimum in the autocorrelation function at ∼50 Å for the apo form compared with that for the holo form). This small difference may be due to the bis-histidyl coordination of the heme cofactor that would be expected to increase the average area/helix in the plane of the monolayer within the hydrophobic domain of the peptide upon axial histidyl ligation and thereby induce a disordering of the helices with the hydrophilic domain of the peptide where there is no such “spacer”. The slightly higher electron density maximum centered at ∼ −15 Å representing the small fraction of helices (∼5%) lying in the plane of the interface remains similar for both apo and heme forms.

Results similar to those described above were obtained upon comparison of the corresponding monolayer electron density profiles for the apo and holo forms of AP2 with the nonbiological Zn33Zn cofactor, as shown in Figure 9a−f. The only small difference with the Zn33Zn cofactor appears to be a somewhat lesser broadening of the interface between the hydrophilic domain of the peptide and the pure aqueous subphase for the holo form (as also evident by comparison of corresponding minimum in the autocorrelation functions of their corresponding gradient electron density profiles at ∼50 Å for the apo and holo forms). This may be due to the much longer Zn33Zn cofactor extending from its axial histidyl ligation within the hydrophobic domain well into the core of the hydrophilic domain, thereby better maintaining the interhelical ordering at the larger area/helix in the plane of the monolayer in the presence of the cofactor.

In Figure 10a−b, we show the monolayer electron density profiles for the apo forms of AP2 as compared with AP3, together with the autocorrelation functions of their corresponding gradient electron density profiles, at a high surface pressure of 55 mN/m. With a large majority of the helices of each peptide oriented approximately perpendicular to the

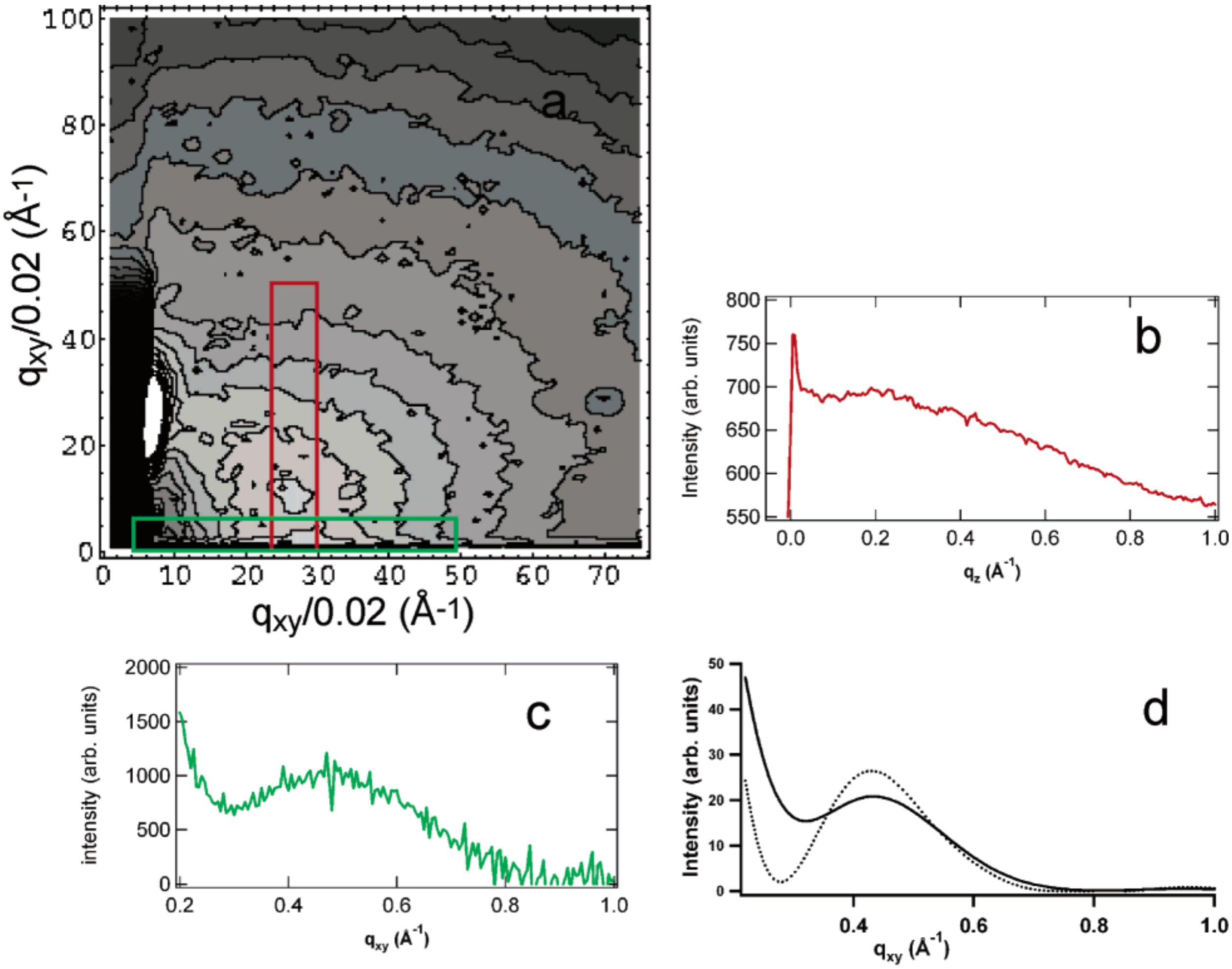

Figure 12. Grazing incidence X-ray diffraction (GIXD) from AP2 peptide monolayers. (a) Contour plot of 2D GIXD collected with a CCD area detector from a monolayer of apo-AP2 at high surface pressure. Integration of the region bounded by the red rectangle along q_{xy} gives the GIXD as a function of q_z (b), including background scattering. Integration of similar data from an apo-AP2 monolayer along the q_z direction (as indicated by the green box), after subtraction of otherwise equivalent GIXD from a monolayer of the phospholipid DGPC, gives the background corrected GIXD as a function of q_{xy} (c). Model calculations for the q_{xy}-dependence of the in-plane diffraction from a bundle of four cylinders (d, dotted curve) show good agreement with the corrected data in (c), especially once the experimental Δq_{xy}-resolution is considered (solid curve).

interface at this high surface pressure, the monolayer electron density profiles over the hydrophobic domain (-20 Å $< z < 0$ Å) are identical, as expected based on their amino acid sequences. The length of their respective hydrophilic domains is seen to differ by ~20 Å, namely, within -50 Å $< z -$ 30 Å, within the monolayer electron density profiles, as also evident in the autocorrelation functions of their respective gradient electron density profiles, which show that the helices of AP2 extend ~20 Å further perpendicular to the interface than those of AP3 (namely, the autocorrelation function for AP3 becomes zero for correlations over distances in excess of 45 Å in the profile, whereas that for AP2 does so only for correlations over distances in excess of 65 Å). This is entirely consistent with the sequences of their respective hydrophilic domains, which differ by 12 residues (namely, 12 residues at 1.5 Å/residue along the axis of an α-helix provides a expected profile length of 18 Å).

The comparisons of the monolayer profile structures for the apo and holo forms of AP2 and AP3 described above indicate that a large majority of the helices of these peptides, namely, about 95%, extend approximately perpendicular to the air−water interface at higher surface pressures, as expected based on their design to form amphiphilic four-helix bundles. Furthermore, the intercalation of the metalloporphyrin (e.g., heme) and Zn33Zn cofactors into the bundles via axial histidyl ligation does not perturb this situation in any substantial way. Overall, each helix of AP2 has 40 residues, which provide a length of ~60 Å for a perfect straight α-helix at 1.5 Å/residue along the long axis. The significant difference between the observed maximum thickness of the monolayer of ~50 Å and the calculated length might be attributed to a uniform tilt of straight α-helices relative to the normal to the plane of the interface of ~33−34°, or the bending of the helices to form a coiled-coil, as would be consistent with their design based on the heptad repeat (see below). Alternatively, a length of ~50 Å for untilted helices would require that the AP2 sequence be only ~83% α-helical, the remainder disordered.

Grazing-incidence X-ray diffraction (GIXD) data from Langmuir monolayers of the amphiphilic peptides apo-AP0 and apo-AP2 at higher surface pressures, where the helices are oriented approximately perpendicular to the monolayer plane, show a broad maximum for momentum transfer parallel to the monolayer plane at $q_{xy} \approx 2\pi/11$ Å^{-1}, which is absent in such data from the aqueous subphase itself and Langmuir monolayers of phospholipids on its surface; for AP0, Figure 11a and c and for AP2, Figure 12a and c. This diffraction arises from the interference between parallel helices. The q_{xy}-dependence of this GIXD data, and its inverse Fourier transform, namely, the in-plane radial autocorrelation function, was modeled approximating the helices as straight rods of uniform electron density of ~8−10 Å diameter. For AP0, the modeling demonstrates that the dihelices aggregate to form four-helix bundles, which are rotationally disordered about the normal to the membrane plane with glasslike interbundle positional ordering in the monolayer plane, Figure 9d. Other possible bundles of the apo-AP0 dihelices can be readily excluded on this basis because their respective GIXD and corresponding radial autocorrelation functions differ qualitatively, well outside the signal-to-noise level, from their experimental counterparts. For apo-AP2, the modeling similarly demonstrates that the single helices aggregate to form four-helix, or possibly 5-helix bundles, Figure 12d. As shown in Figures 11d and 12d, allowing for the finite Δq_{xy}-resolution provides near perfect agreement between the q_{xy}-dependence of the calculated GIXD for a four-helix bundle of ~9-Å-diameter helices at a ~10-Å inter-helix separation in the plane perpendicular to the bundle long-axis for AP0, and of ~10-Å-diameter helices at a ~12-Å inter-helix separation for AP2, and those measured experimentally (Figures 11c and 12c, respectively). The q_z-dependence of the GIXD data for both peptides has a primary maximum at $q_z = 0$ Å^{-1} and a weaker secondary maximum for $q_z > 0$ Å^{-1} at $q_z \approx 0.20-0.25$ Å^{-1}. The absence of any other maximum at larger values of q_z rules out the possibility of straight α-helices uniformly tilted by as much as ~33−34°. Instead, the GIXD data can be analyzed in terms of Crick's analysis of the Fourier transform of coiled-coils,[19,20] consistent with their design based on the heptad repeat. Assuming that the secondary maximum off the q_{xy}-axis for $q_z > 0$ Å^{-1} for both AP0 and AP2 which occurs at $q_z \approx 0.20-0.25$ Å^{-1} to be the first observable layer line from a coiled-coil indicates, for a four-helix bundle, that the pitch of the major helix is ~100−125 Å with a pitch angle of ~14−17°. This pitch angle would reduce the length of the helices projected onto the bundle axis normal to the monolayer plane by only ~3 Å, namely, from ~60 to ~57 Å, still substantially longer than the length of ~50 Å indicated by the electron density profiles. This result further suggests that the AP2 sequence is not fully α-helical, namely, only ~88% allowing for the ~3-Å reduction in projected length of the helices onto the bundle axis because of the pitch angle of their coiled-coil structure.

In conclusion, we have successfully designed and characterized amphiphilic four-helix bundle peptides that are capable of binding metalloporphyrin prosthetic groups within their hydrophilic domains and both metalloporphyrin and bacteriochlorophylls within their hydrophobic domains with relatively high affinities. The specificity of the hydrophobic domain of AP2 for bacteriochlorophylls may allow the specific binding of metal-porphyrins within its hydrophilic domain when a metal-bacteriochlorophyll already occupies the binding site in its hydrophobic domain. In addition, the AP0 and AP2 peptides are capable of binding nonbiological prosthetic groups containing extended π-electron systems via axial histidyl coordination at a single site within their hydrophilic or hydrophobic domain, respectively. Related prosthetic groups can exhibit electric charge separation over large distances within the conjugated bis(porphyrin) itself, as oriented within the core of the bundle. Approaches with either cofactor-to-cofactor electron transfer or intra-prosthetic-group electron transfer permit vectorial light-induced electron transfer from the electron donor to the acceptor across the interface between polar and nonpolar media.

Acknowledgment. We thank Andrey Tronin for assistance with data collection, Mike Sullivan for use of the support lab at beamline X9, and Benjamin M. Ocko, Elaine DiMasi, and Scott Coburn for technical assistance at beamline X22-B at the National Synchrotron Light Source, Brookhaven National Laboratory (NSLS/BNL). This work was supported by the MRSEC Program of the National Science Foundation under award no. DMR96-32598, the Biomolecular Materials Program in the Materials Science & Engineering Division of the U.S. Department of Energy under grant no. DE-FG02-04ER46156, and the National Institutes of Health under grants GM48130, GM41048, GM63388, GM55876, GM071628, and RR14812. The NSLS/BNL and APS/ANL are supported by the U.S. Department of Energy.

Supporting Information Available: We present the synthesis of Zn33Zn in detail and provide references to publications describing the other methods employed in this work. This material is available free of charge via the Internet at http://pubs.acs.org.

References

(1) Robertson, D. E.; Farid, R. S.; Moser, C. C.; Urbauer, J. L.; Mulholland, S. E.; Pidikiti, R.; Lear, J. D.; Wand, A. J.; Degrado, W. F.; Dutton, P. L. *Nature* **1994**, *368*, 425−431.
(2) Cochran, F. V.; Wu, S. P.; Wang, W.; Nanda, V.; Saven, J. G.; Therien, M. J.; DeGrado, W. F. *J. Am. Chem. Soc.* **2005**, *127*, 1346−1347.
(3) Shifman, J. M.; Gibney, B. R.; Sharp, R. E.; Dutton, P. L. *Biochemistry* **2000**, *39*, 14813−14821.
(4) Chen, X. X.; Moser, C. C.; Pilloud, D. L.; Dutton, P. L. *J. Phys. Chem. B* **1998**, *102*, 6425−6432.
(5) Strzalka, J.; Chen, X. X.; Moser, C. C.; Dutton, P. L.; Ocko, B. M.; Blasie, J. K. *Langmuir* **2000**, *16*, 10404−10418.
(6) Strzalka, J.; Chen, X. X.; Moser, C. C.; Dutton, P. L.; Bean, J. C.; Blasie, J. K. *Langmuir* **2001**, *17*, 1193−1199.
(7) Ye, S. X.; Strzalka, J. W.; Discher, B. M.; Noy, D.; Zheng, S. Y.; Dutton, P. L.; Blasie, J. K. *Langmuir* **2004**, *20*, 5897−5904.
(8) Discher, B. M.; Noy, D.; Strzalka, J.; Ye, S. X.; Moser, C. C.; Lear, J. D.; Blaise, J. K.; Dutton, P. L. *Biochemistry* **2005**, *44*, 12329−12343.
(9) Huang, S. S.; Koder, R. L.; Lewis, M.; Wand, A. J.; Dutton, P. L. *Proc. Natl. Acad. Sci. U.S.A.* **2004**, *101*, 5536−5541.
(10) Xia, D.; Yu, C. A.; Kim, H.; Xian, J. Z.; Kachurin, A. M.; Zhang, L.; Yu, L.; Deisenhofer, J. *Science* **1997**, *277*, 60−66.

(11) Hartwich, G.; Fiedor, L.; Simonin, I.; Cmiel, E.; Schafer, W.; Noy, D.; Scherz, A.; Scheer, H. *J. Am. Chem. Soc.* **1998**, *120*, 3675−3683.
(12) Noy, D.; Fiedor, L.; Hartwich, G.; Scheer, H.; Scherz, A. *J. Am. Chem. Soc.* **1998**, *120*, 3684−3693.
(13) Noy, D.; Discher, B. M.; Rubtsov, I. V.; Hochstrasser, R. M.; Dutton, P. L. *Biochemistry* **2005**, *44*, 12344−12354.
(14) Redmore, N. P.; Rubtsov, I. V.; Therien, M. J. *J. Am. Chem. Soc.* **2003**, *125*, 8769−8778.
(15) Anderson, H. L. *Inorg. Chem.* **1994**, *33*, 972−981.
(16) Lin, V. S. Y.; Therien, M. J. *Chem.*−*Eur. J.* **1995**, *1*, 645−651.
(17) Shediac, R.; Gray, M. H. B.; Uyeda, H. T.; Johnson, R. C.; Hupp, J. T.; Angiolillo, P. J.; Therien, M. J. *J. Am. Chem. Soc.* **2000**, *122*, 7017−7033.
(18) Battistuzzi, G.; Borsari, M.; Cowan, J. A.; Ranieri, A.; Sola, M. *J. Am. Chem. Soc.* **2002**, *124*, 5315−5324.
(19) Crick, F. H. C. *Acta Crystallogr.* **1953**, *6*, 685−689.
(20) Crick, F. H. C. *Acta Crystallogr.* **1953**, *6*, 689−697.

NL050542K